Electronic Supplementary Information (ESI)

Solvent Vapour Annealing of Methylammonium Lead Halide Perovskite: What's the catch?

Onkar S. Game[a], Joel A. Smith[a], Tarek I. Alanazi[a], Michael Wong-Stringer[a], Vikas Kumar[b], Cornelia Rodenburg[b], Nick J. Terrill[c] and David G. Lidzey[a]**

a. Department of Physics and Astronomy, University of Sheffield, Sheffield, U.K.
b. Department of Material Science and Engineering, University of Sheffield, Sheffield, UK
c. Diamond Light Source Ltd, Diamond House, Harwell Science & Innovation Campus, Didcot Oxfordshire, U.K.

*Correspondane: o.game@sheffield.ac.uk, d.g.lidzey@sheffield.ac.uk

ESI Note 1: PbI_2 crystallization

The crystallization behaviour of PbI_2 and its location in mixed-phase perovskite films is a matter of ongoing research within the field. Most of the reports using ACN/MA solvent system for PbI_2-excess compositions demonstrate the crystallization of PbI_2 as phase-separated grains or segregated regions in the films[1, 2]. However, we believe that this behaviour is not specific to the ACN/MA solvent system. Some of the early reports on PbI_2 excess in $MAPbI_3$ claimed a uniform distribution of PbI_2 around grain boundaries[3]. However, recent reports on excess-PbI_2 in precursor solutions made with DMF/DMSO[4-6] or GBL/DMSO[7] solvents also showed crystallization of PbI_2 grains, distributed throughout the film. We believe that such differences could have their origin in different annealing temperatures and durations, solvent ratios, fabrication environment (air vs nitrogen) and occasionally in batch-to-batch variation.

References:

1. D. P. McMeekin, S. Mahesh, N. K. Noel, M. T. Klug, J. Lim, J. H. Warby, J. M. Ball, L. M. Herz, M. B. Johnston and H. J. Snaith, *Joule*, 2019, **3**, 387-401.
2. A. J. Ramadan, N. K. Noel, S. Fearn, N. Young, M. Walker, L. A. Rochford and H. J. Snaith, *Chemistry of Materials*, 2018, **30**, 7737-7743.
3. C. Roldán-Carmona, P. Gratia, I. Zimmermann, G. Grancini, P. Gao, M. Graetzel and M. K. Nazeeruddin, *Energy & Environmental Science*, 2015, **8**, 3550-3556.
4. J.-a. Yang, A. Xiao, L. Xie, K. Liao, X. Deng, C. Li, A. Wang, Y. Xiang, T. Li and F. Hao, *Electrochimica Acta*, 2020, **338**, 135697.
5. J. Euvrard, O. Gunawan and D. B. Mitzi, *Advanced Energy Materials*, 2019, **9**, 1902706.
6. N. Pant, A. Kulkarni, M. Yanagida, Y. Shirai, T. Miyasaka and K. Miyano, *Advanced Materials Interfaces*, 2019, **7**, 1901748.
7. J. Chang, H. Zhu, J. Xiao, F. H. Isikgor, Z. Lin, Y. Hao, K. Zeng, Q.-H. Xu and J. Ouyang, *Journal of Materials Chemistry A*, 2016, **4**, 7943-7949.

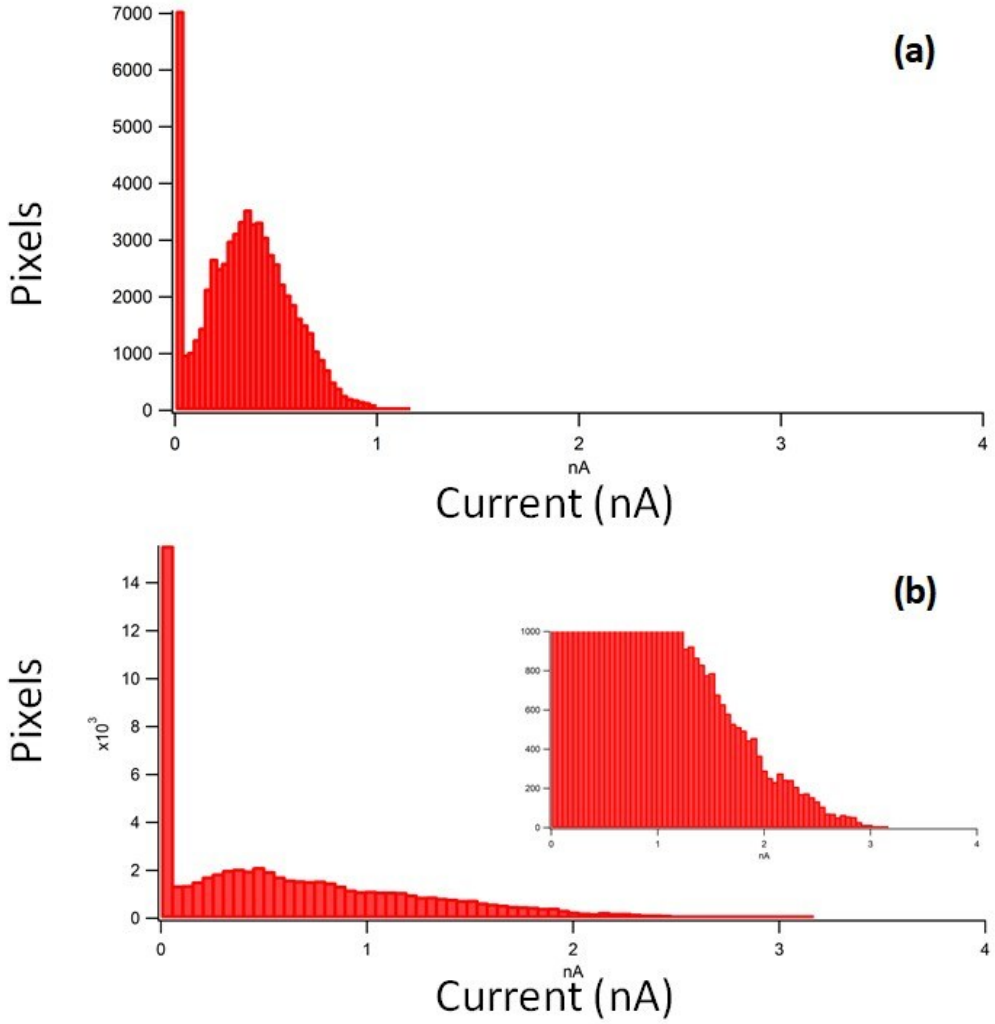

Fig S1 (a) and **(b)** show histogram of pixel frequency vs photocurrent for Pb-NVA and Pb-VA pc-AFM map in Fig 1(b) and (d) respectively. Inset of Fig S1 (b) shows the magnified view of Pb-VA histogram indicating presence of pixels (regions/grains) with photocurrent magnitude higher than 1 nA.

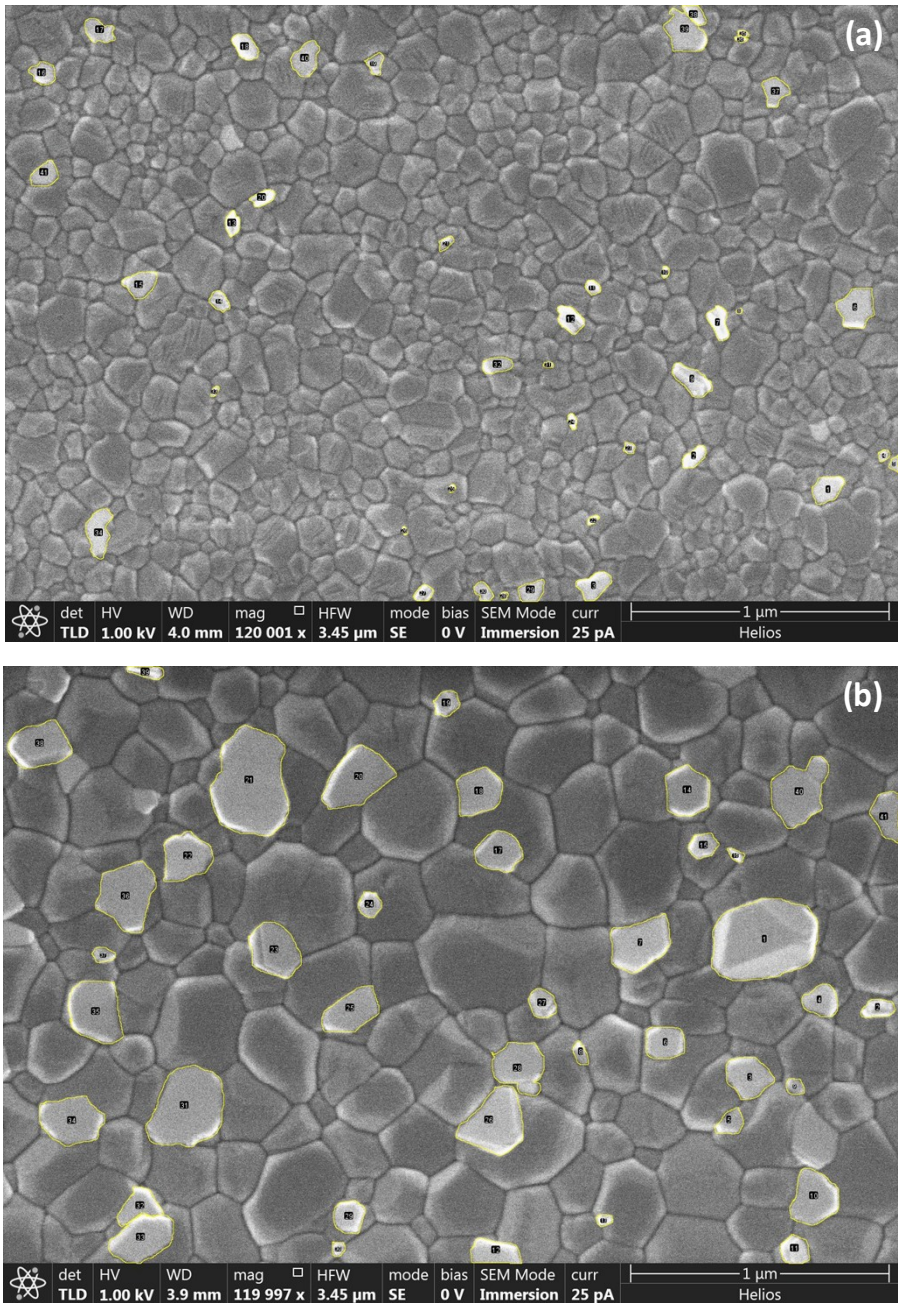

Fig S2 The total areas occupied by grains showing brighter contrast (highlighted in yellow) than surrounding grains in SEM images (with a total area of 8.02 μm^2) were calculated using ImageJ software. These bright contrast PbI_2-rich grains occupied ~ 0.22 μm^2 area in the SEM image of (a) Pb-NVA (3% of the surface) which on solvent vapour annealing increased to ~ 1.04 μm^2 for (b) Pb-VA (13% of the surface).

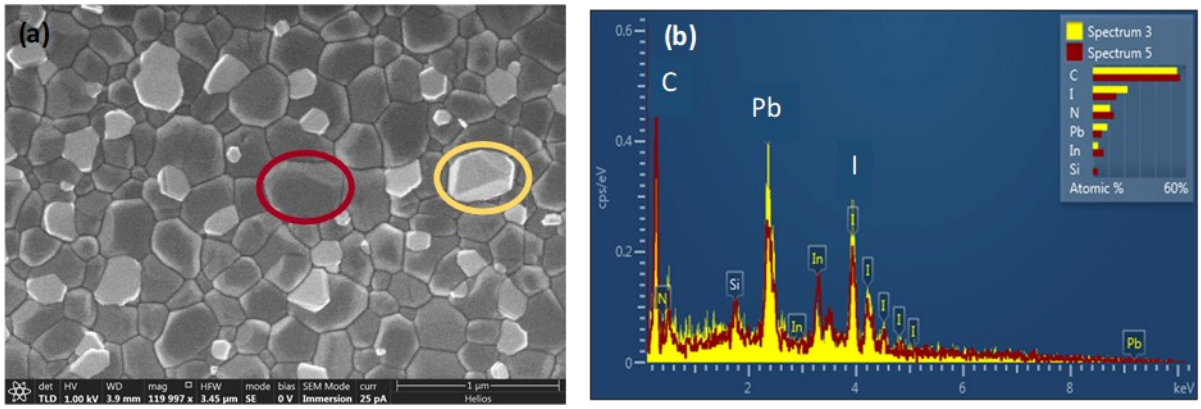

Fig S3 (a) shows the SEM of PbI_2 excess solvent vapour annealed (Pb-VA) film. Representative grains with dark and bright contrast are marked in red and yellow circles respectively. (b) shows the point EDS spectra of Pb-VA film at two locations marked red and yellow in (a).

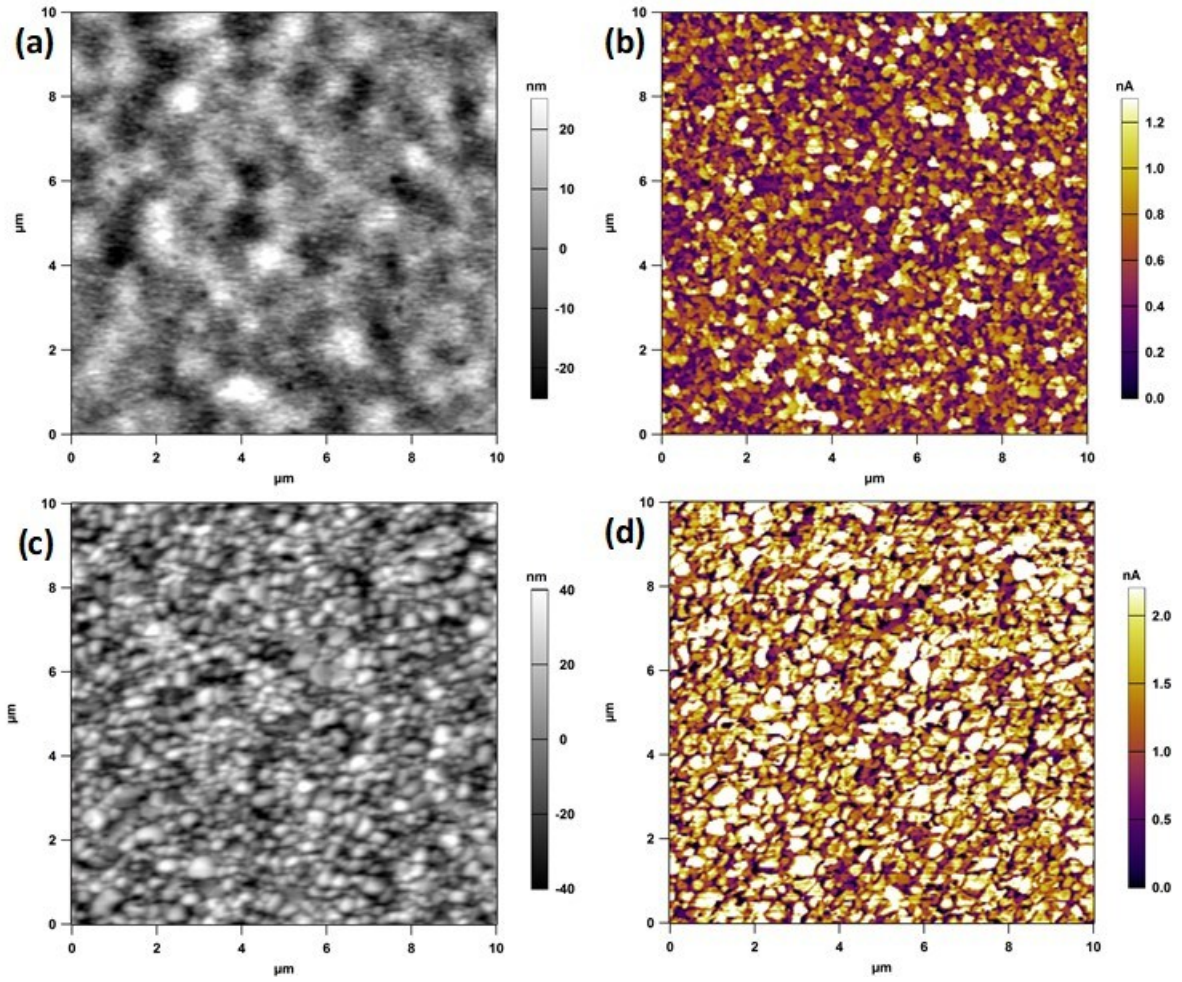

Fig S4 (a) and **(c)** shows the contact mode AFM (height profile) for MA-NVA and MA-VA films 10 µm × 10 µm scan; **(b)** and **(d)** show photocurrent maps (10 µm × 10 µm) simultaneously acquired with topography using pc-AFM under illumination for Pb-NVA and Pb-VA respectively.

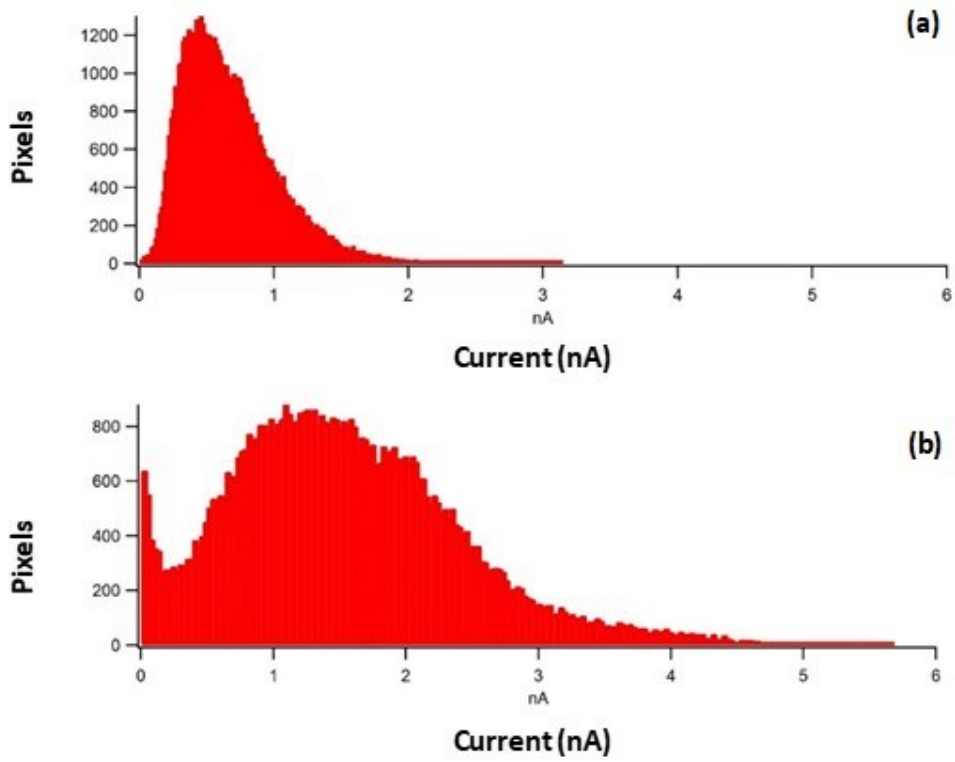

Fig S5 (a) and **(b)** show histogram of pixels vs photocurrent in pc-AFM map (Fig 3 (b), (d)) for MA-NVA and MA-VA films respectively.

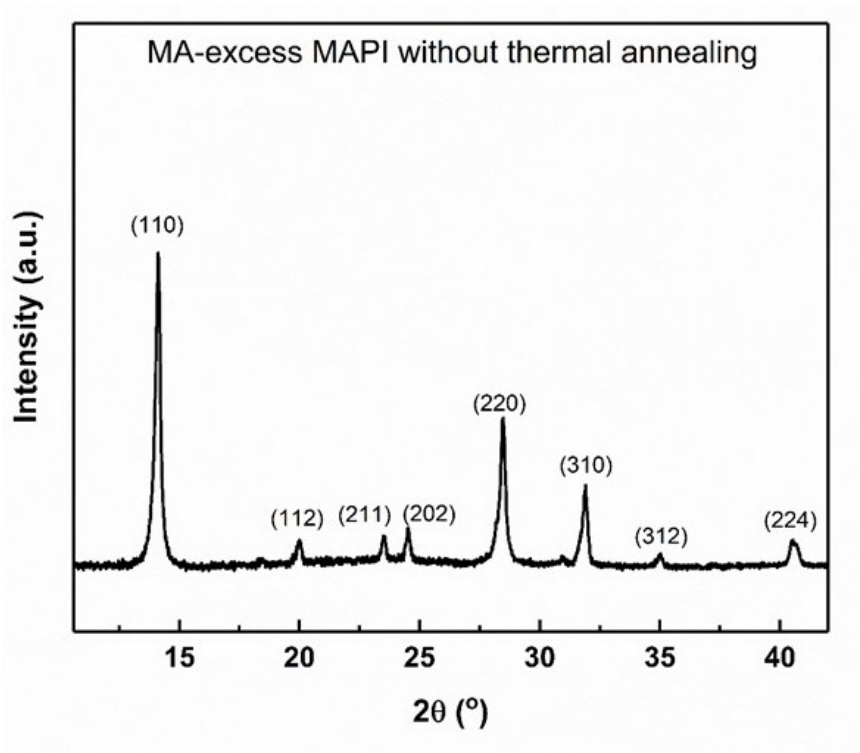

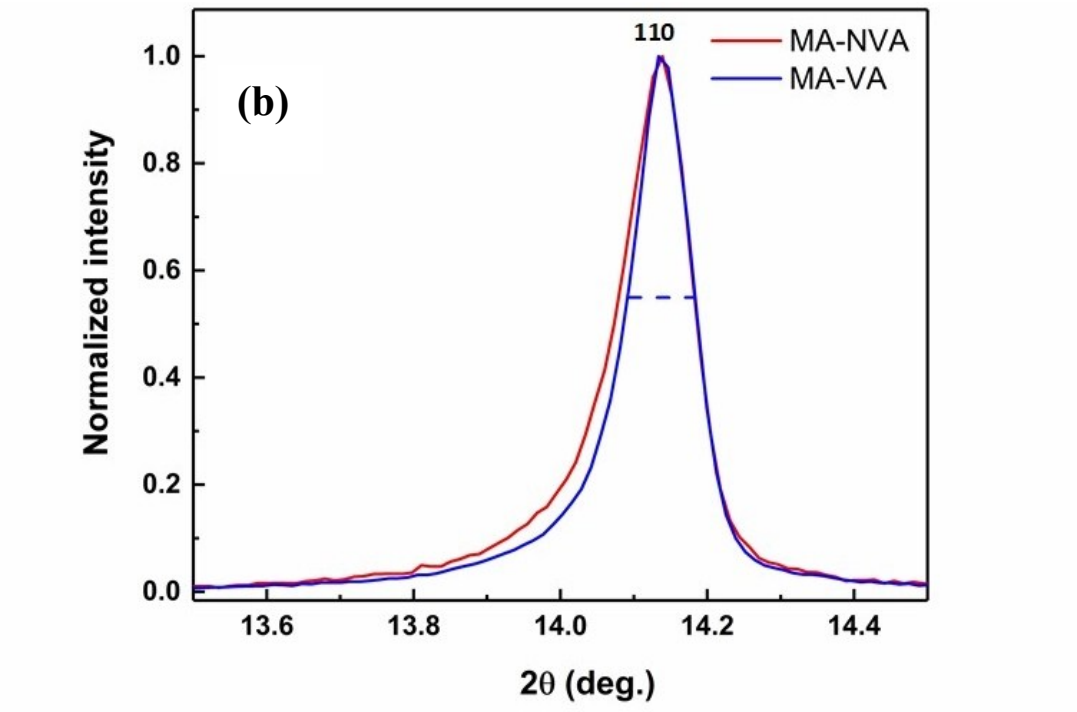

Fig S6 (a) XRD of as spin cast MAI excess $MAPbI_3$ without any thermal or solvent treatment. **(b)** Normalized (110) XRD peak of MA-NVA and MA-VA showing reduced FWHM in MA-VA implying grain growth post solvent vapour annealing.

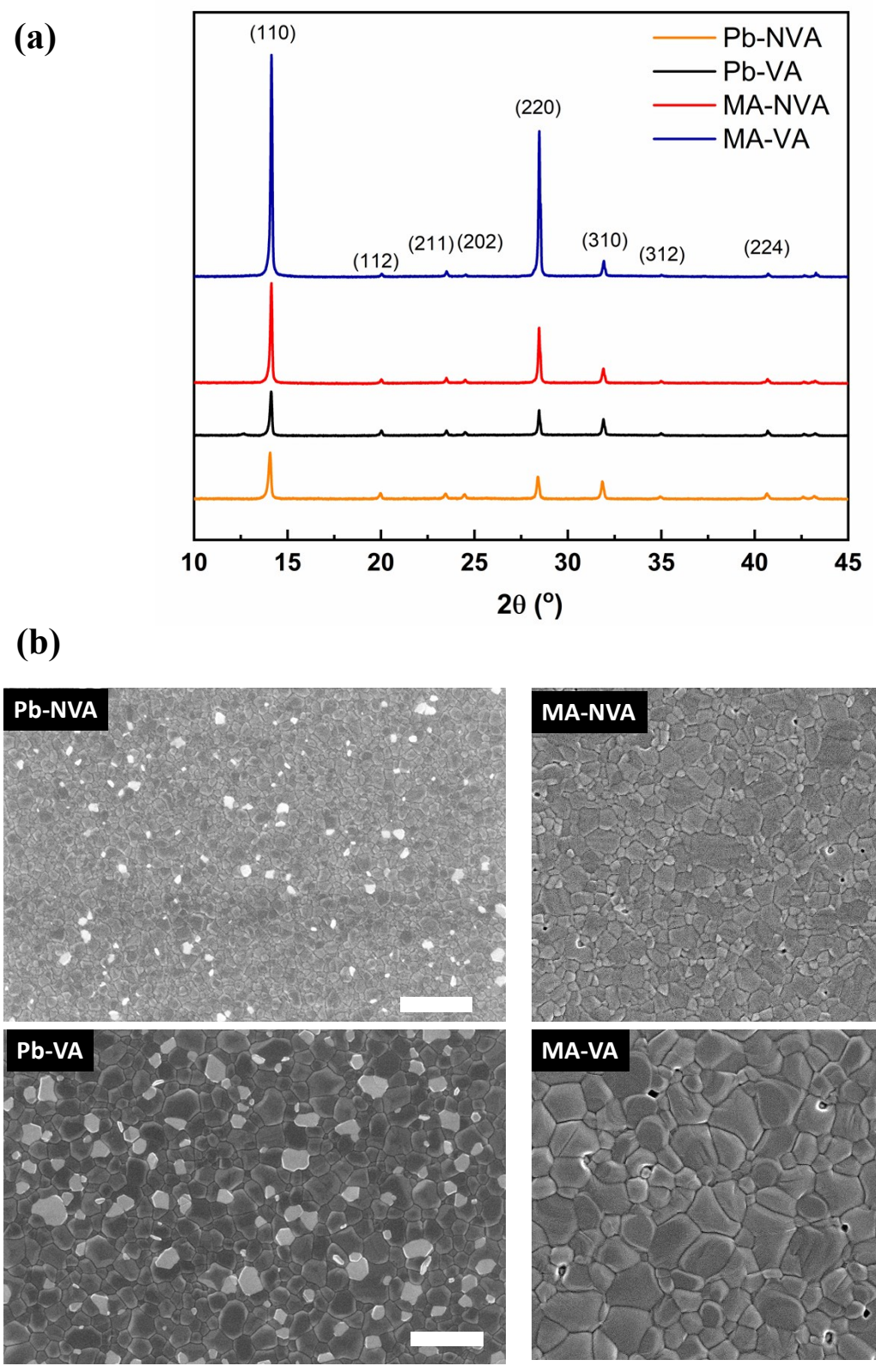

Fig S7 (a) XRD of PbI_2-excess and MAI-excess compositions with and without solvent vapour annealing. **(b)** SEM of .PbI_2-excess and MAI-excess compositions with and without solvent vapour annealing. In all cases, the scale bar represents 1 µm.

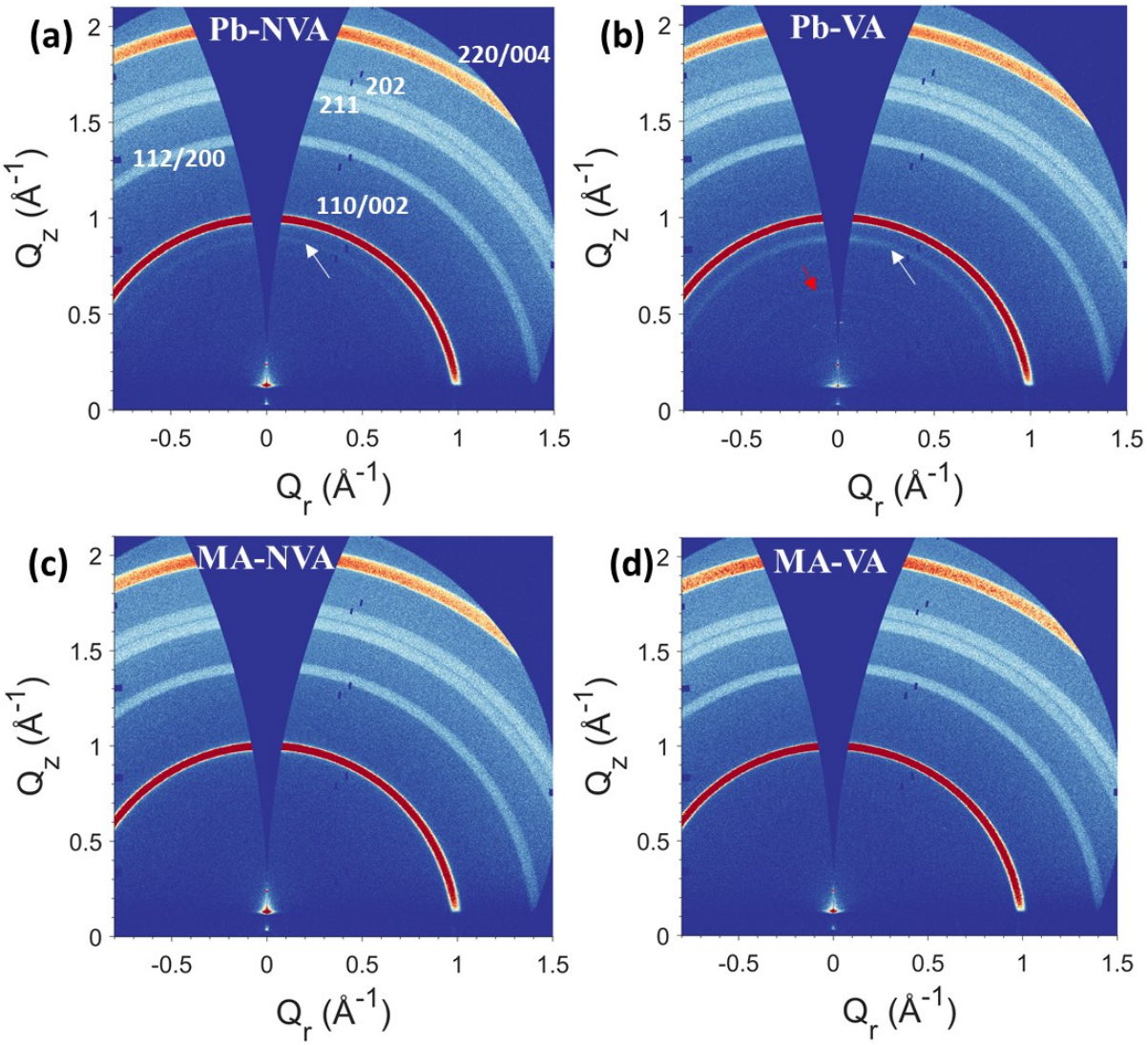

Fig S8 Grazing incidence (1.5°) wide angle X-ray scattering 2D patterns collected for a) Pb-NVA, b) Pb-VA, c) MA-NVA and d) MA-VA films. Here, scatter from PbI_2 is indicated by a white arrow in the PbI_2 excess samples. The red arrow shows additional weakly scattering features at low Q (or low 2θ) for Pb-VA.

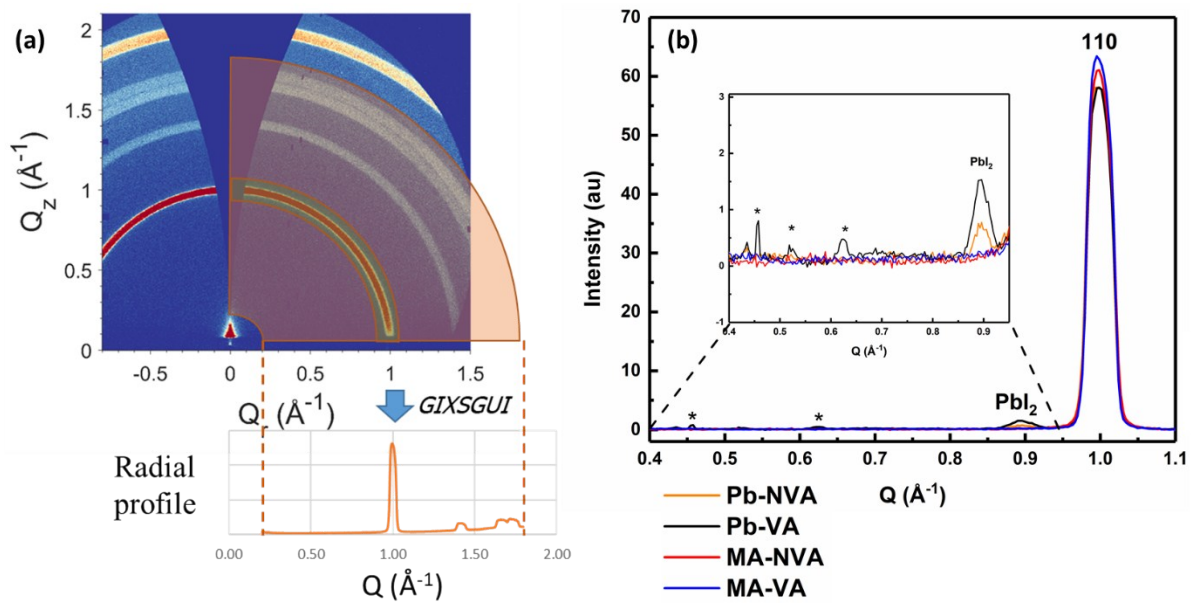

Fig S9 (a) Schematic of the reduction of the 2D detector scattering patterns to a radial profile of azimuthally integrated intensity data (integrated for all χ as a function of Q), also known as a 'cake remapping'. (b) 1D radial profiles for all samples obtained after azimuthal integration of 2D patterns in Fig S8 (a) – (d). Inset shows the magnified view of 1D radial profile in the range of Q = 0.4 to 0.95 $Å^{-1}$ (equivalent to 2θ = 5.6° to 13.5°).

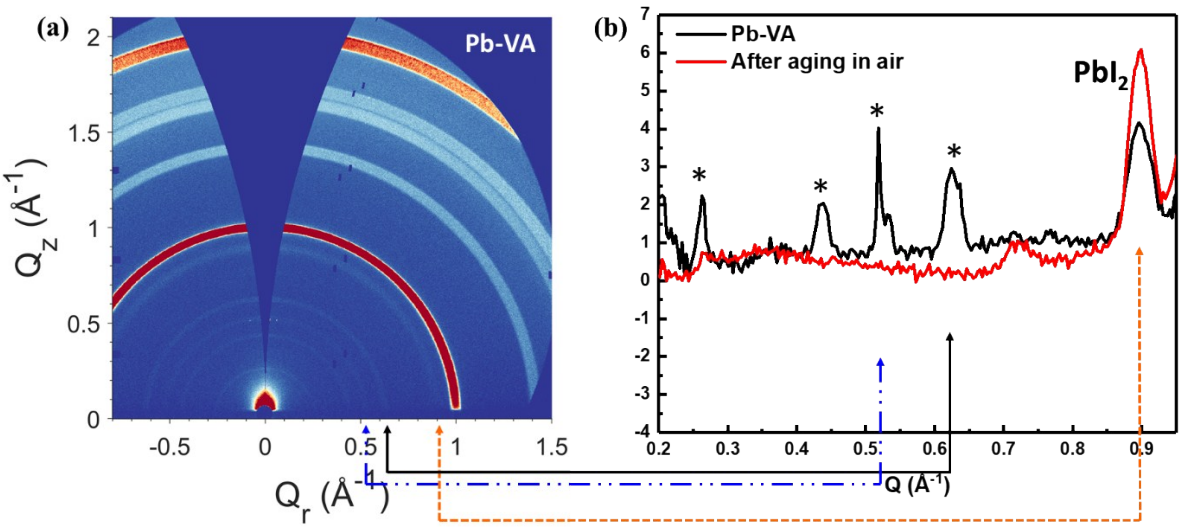

Fig S10 (a) Extended accumulation grazing incidence (0.5°) wide angle X-ray 2D scattering pattern of PbI_2 excess solvent vapour annealed film. (b) 1D radial profile of 2D pattern in the range of Q = 0.2 to 0.95 Å^{-1}, showing crystalline PbI_2 and additional peaks at low Q marked with asterisks (*). These features were no longer present after overnight storage in ambient air, as shown in the radial profile for an aged sample (red). We also observed a small increase in the PbI_2 scattering signal; a finding consistent with our proposed mechanism shown in Fig 9 of the main paper.

Composition	Device code	Scan	Voc (V)	Jsc (mA/cm^2)	FF(%)	Eff(%)
Pb excess	**Pb-NVA**	Fw	1.06	20.30	57.2	12.3
		Rev	**1.07**	**20.40**	**73.6**	**16.0**
Pb excess	**Pb-VA**	Fw	1.01	20.32	33.7	6.91
		Rev	**1.06**	**20.18**	**74.1**	**15.8**
Stoichiometric	**MAPI-NVA**	Fw	1.06	20.7	70.5	15.5
		Rev	**1.07**	**20.7**	**77.2**	**17.1**
Stoichiometric	**MAPI-VA**	Fw	1.03	20.54	64.2	13.6
		Rev	**1.05**	**20.51**	**76.3**	**16.4**
MAI-excess	**MA-NVA**	Fw	1.10	20.98	70.2	16.2
		Rev	**1.10**	**21.00**	**77.2**	**17.8**
MAI-excess	**MA-VA**	Fw	1.07	20.93	71.0	15.9
		Rev	**1.09**	**20.91**	**77.8**	**17.7**

Table S1 Photovoltaic parameters of best devices for each case. –NVA and –VA stand for non-vapour annealed and vapour annealed respectively. Pb-, MA- and MAPI- compositions correspond to lead excess, MAI excess and stoichiometric $MAPbI_3$ respectively.

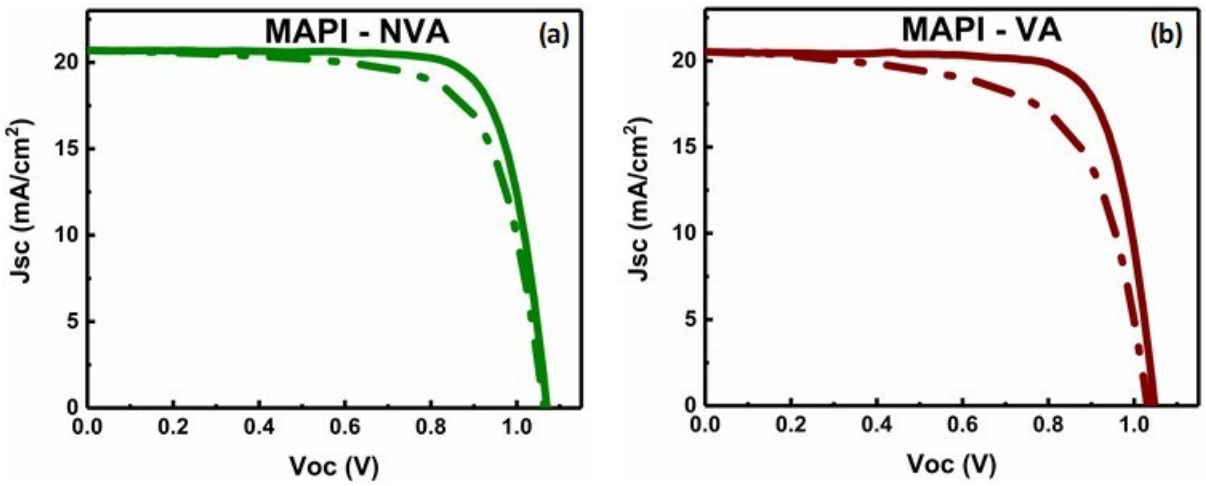

Fig S11 J-V curves of stoichiometric (MAI:PbI_2 = 1:1) $MAPbI_3$ based devices (a) without and (b) with solvent-vapour annealing.

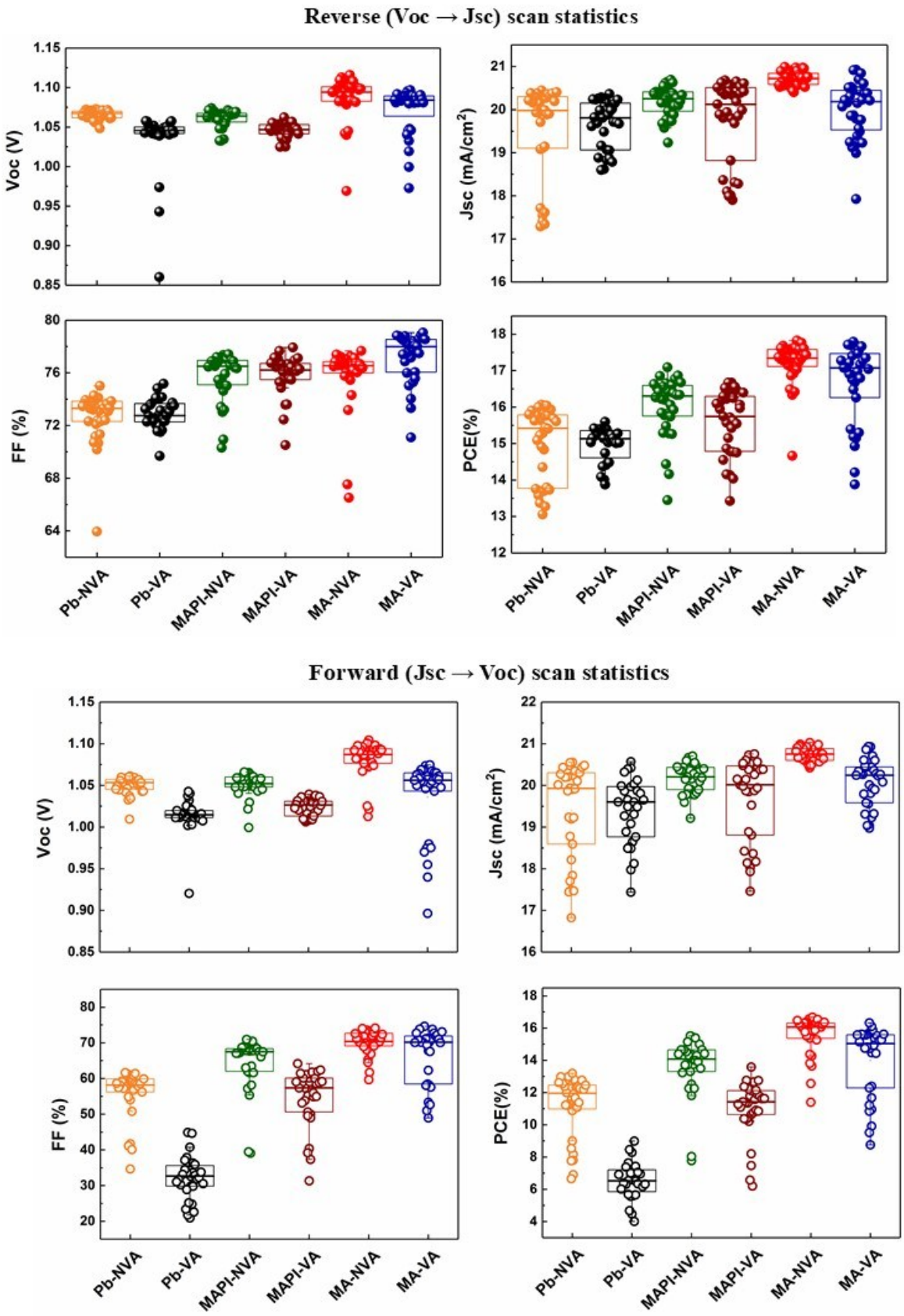

Fig S12 Reverse and forward scan statistic of lead excess (Pb-), stoichiometric (MAPI-) and MAI excess (MA-) compositions in planar architecture without (-NVA) or with (-VA) solvent vapour annealing. Horizontal line in the box shows the median value.

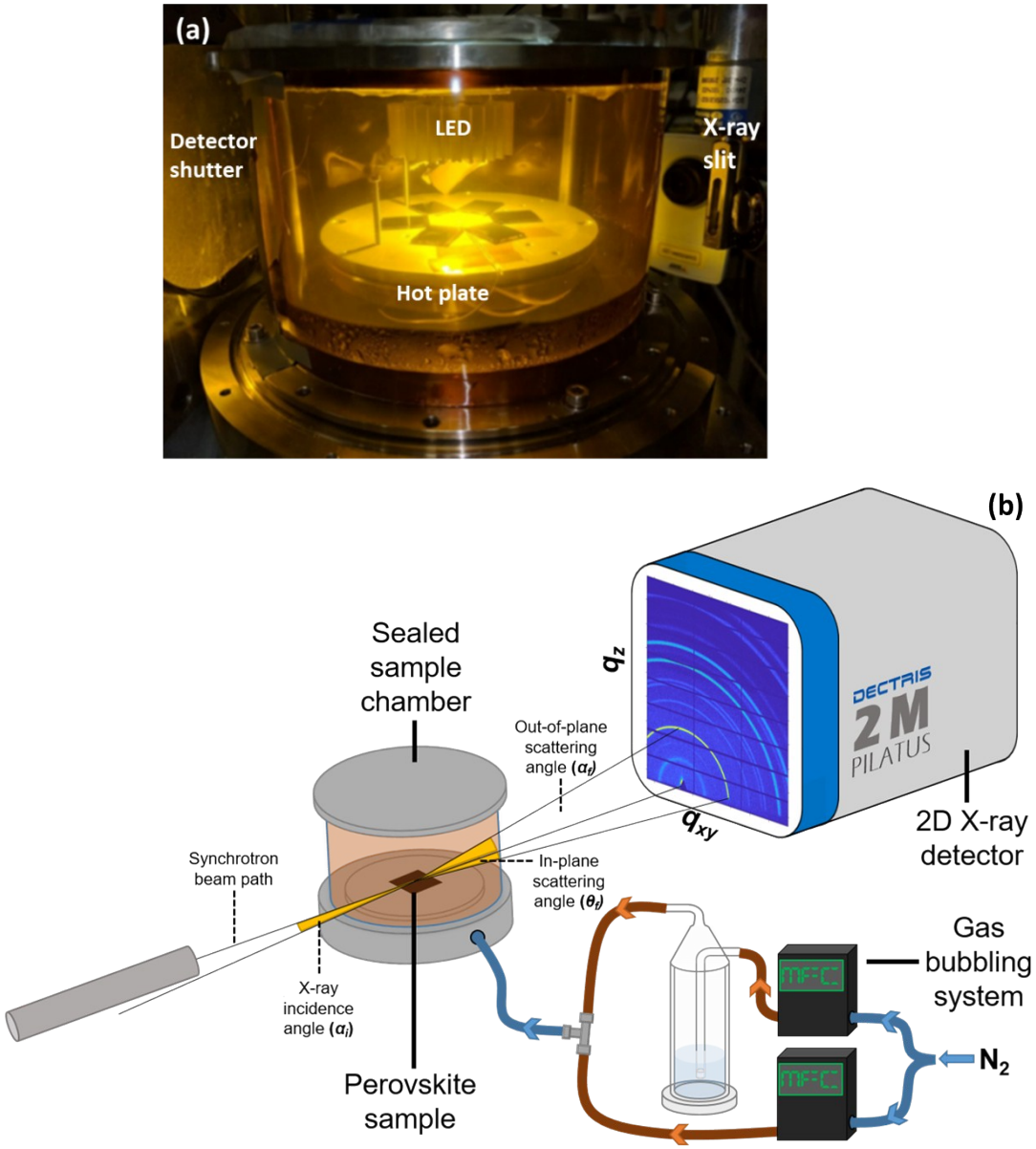

Fig S13 (a) Photograph of moisture chamber that was used to study degradation using *in situ* GIWAXS measurements on perovskite films. The chamber walls were composed of a thick Kapton film that is transparent to X-rays. (b) Schematic of the *in situ* GIWAXS measurements performed at the Diamond Light Source I22 synchrotron beamline with an X-ray beam energy set at 10 keV. Here the beam was incident at 0.3° with scattered X-rays detected using a Pilatus P3-2M detector.

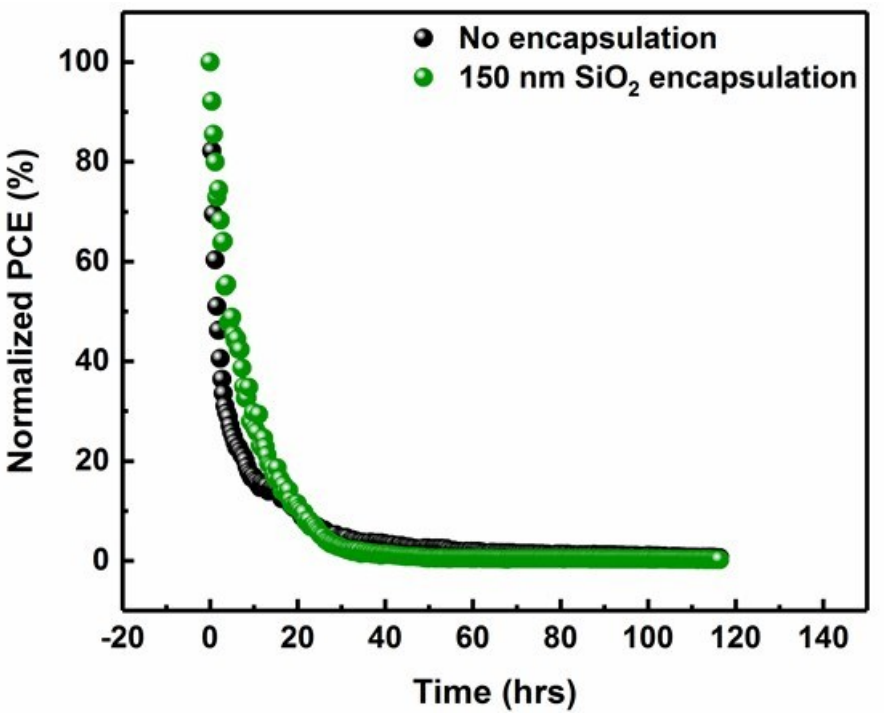

Fig S14 Continuous illumination device lifetime (PCE vs time) of Pb-excess solvent vapour annealed (Pb-VA) composition without (black) and with (green) 150 nm SiO_2 encapsulation.

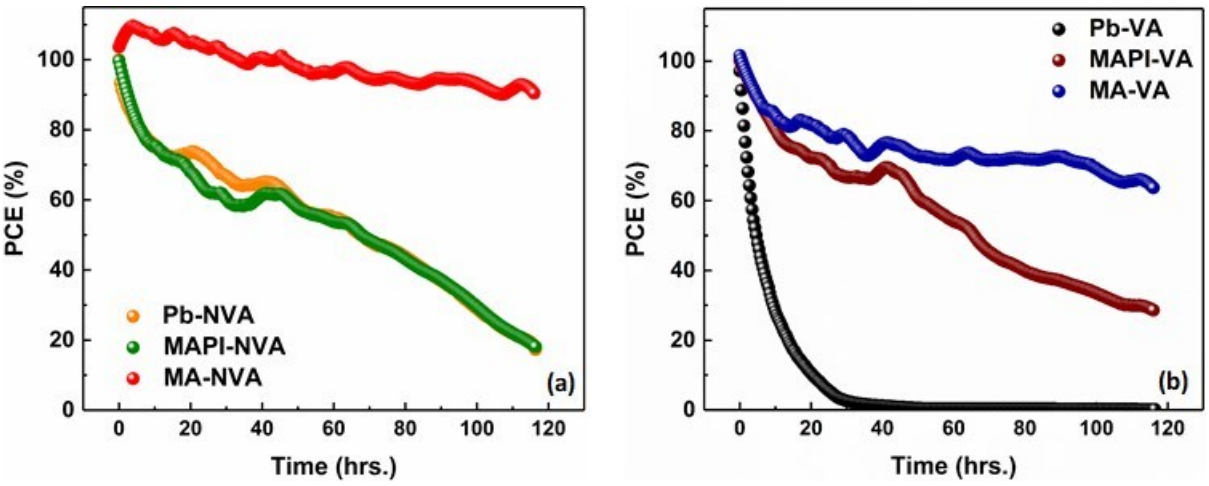

Fig S15 Composition dependence of continuous illumination device lifetimes (PCE vs time) (a) without and (b) with solvent vapour annealing. Compositions are abbreviated as Pb-excess (Pb-), Stoichiometric (MAPI-) and MA-excess (MA-).

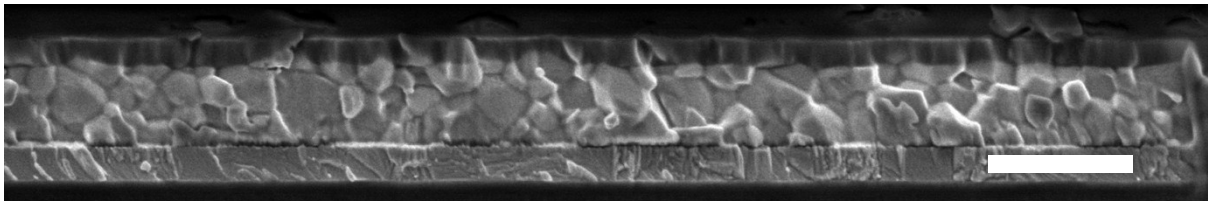

Fig S16 Representative device cross-section of 6% PbI_2-excess (Pb-NVA) device before subjecting to 120 hrs lifetime testing. The grain structure within the perovskite film is well defined, with grain sizes ranging from 100 – 300 nm. Scale bar is 500 nm.

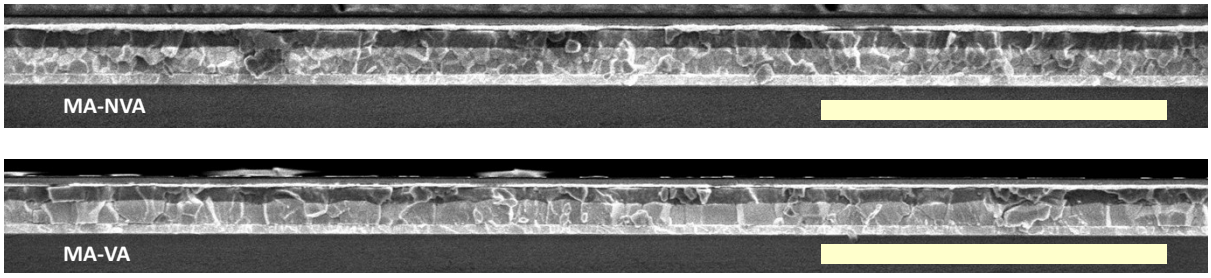

Fig S17 Cross-sectional SEM images of MA-NVA and MA-VA on a wide scale (Scale bar: 4 µm). MA-NVA did not show any voids at the ETL-perovskite interface, implying good mechanical contact between the perovskite film and ETL. This behaviour persisted even after solvent vapour annealing as evident from the cross-sectional SEM of MA-VA.

Scheme S18: Degradation pathways in PbI_2-excess perovskite devices under illumination[8, 9]

1. Under illumination, the excess PbI_2 undergoes photodecomposition process according to

$$excess\ PbI_2 \xrightarrow{h\vartheta} Pb(0) + I_2\ (g)$$

2. Iodine gas formed in process 1 undergoes atomic iodide generation[6] under illumination

$$I_2 \xrightarrow{h\vartheta} 2I^{\circ}$$

3. Atomic iodine reacts with mobile iodide species (I^-) from $MAPbI_3$

$$2I^- + 2I^{\circ} \xrightarrow{h\vartheta} 2\ I^{\circ}{}_2^-$$

4. Mobile MA+ (CH_3NH_3+) ions react with $I^{\circ}{}_2^-$ species to form gaseous methylamine (CH_3NH_2), iodine (I_2) and hydrogen (H_2)

$$2CH_3NH_3{}^+ + 2\ I^{\circ}{}_2^- \xrightarrow{h\vartheta} 2CH_3NH_2 + 2I_2 + H_2$$

References for Scheme S18:

8 E. J. Juarez-Perez, L. K. Ono, M. Maeda, Y. Jiang, Z. Hawash and Y. Qi, *Journal of Materials Chemistry A*, 2018, **6**, 9604-9612.

9. S. Wang, Y. Jiang, Emilio J. Juarez-Perez, Luis K. Ono and Y. Qi, *Nat Energy*, 2016, **2**, 16195.